The role of boundary variability in polycrystalline grain-boundary diffusion

M. M. Moghadam, J. M. Rickman, M. P. Harmer, and H. M. Chan

Articles you may be interested in

Role of segregating impurities in grain-boundary diffusion
J. Chem. Phys. **126**, 094707 (2007); 10.1063/1.2672993

The effect of strong surface energy anisotropy on migrating grain-boundary grooves
J. Appl. Phys. **100**, 053523 (2006); 10.1063/1.2336980

Impact of microstructure on grain-boundary diffusion in polycrystals
J. Appl. Phys. **98**, 063511 (2005); 10.1063/1.2043257

Fast grain boundary diffusion and rate-limiting surface exchange reactions in polycrystalline materials
J. Appl. Phys. **97**, 093504 (2005); 10.1063/1.1882770

Formation of porous grain boundaries in polycrystalline silicon thin films
J. Appl. Phys. **91**, 9408 (2002); 10.1063/1.1476088

The role of boundary variability in polycrystalline grain-boundary diffusion

M. M. Moghadam, J. M. Rickman, M. P. Harmer, and H. M. Chan
Department of Materials Science and Engineering, Lehigh University, Bethlehem, Pennsylvania 18015, USA

We investigate the impact of grain-boundary variability on mass transport in a polycrystal. More specifically, we perform both numerical and analytical studies of steady-state diffusion in prototypical microstructures in which there is either a discrete spectrum of grain-boundary activation energies or else a complex distribution of grain-boundary character, and hence a continuous spectrum of boundary activation energies. An effective diffusivity is calculated for these structures using simplified multi-state models and, for the case of a continuous spectrum, employing experimentally obtained grain-boundary energy data. We identify different diffusive regimes for these cases and quantify deviations from Arrhenius behavior using effective medium theory. Finally, we examine the diffusion kinetics of a simplified model of an interfacial layering (i.e., complexion) transition. © 2015 AIP Publishing LLC. [http://dx.doi.org/10.1063/1.4906778]

I. INTRODUCTION

Most models of grain-boundary (GB) diffusion in polycrystals assume, for tractability, that all boundaries have identical diffusivities and, hence, the same activation energies for diffusion. For all but the simplest of microstructures, the reality is, of course, much more complex. In particular, GB character is inherently variable,[1] and therefore there is a spectrum of diffusivities associated with the boundaries that comprise a polycrystal. Moreover, there is accumulating evidence that layering (i.e., complexion) transitions[2,3] can occur at grain boundaries as a function of temperature or pressure, thereby altering boundary structure and chemistry and, therefore, boundary kinetics. The interplay among these factors in systems with interconnected GB networks makes the determination of the effective diffusion response for polycrystals non-trivial in many cases. In particular, the effective activation energy may be a function of temperature and will be dictated by a complicated microstructural average.

A number of simplified models of polycrystalline mass transport in idealized geometries have been formulated and quantitative results have been obtained in certain diffusive regimes. For example, Whipple and Suzuoka considered an isolated, isotropic GB region with a high diffusivity surrounded by a lower diffusivity bulk region and were able to obtain approximate, analytical solutions to the diffusion equation.[4,5] These solutions can be applied to the description of polycrystalline diffusion in the case of well-separated boundaries (i.e., large grain size) and small bulk diffusion lengths (i.e., type-B diffusion kinetics).[6] More recently, this analysis has been generalized to the case of thin films by Gilmer and Farrell.[7,8] Moreover, Fisher[9] also employed an idealized representation of an isolated grain boundary to obtain the concentration profile in the boundary when there is a constant surface source, neglecting volume diffusion from that source. As the aforementioned models are based on structureless boundaries, other workers[10] have extended these treatments by incorporating more realistic descriptions of low-angle boundary structure in diffusive models based on dislocation arrays. In addition, others have sought to include microstructural features of

a polycrystal in their analysis,[11,12] and to formulate numerical models of non-steady state diffusion in idealized polycrystals.[13]

In recent years, some investigators have begun to examine the role of GB variability in the context of diffusion in polycrystalline media. For example, Chen and Schuh[14] have modeled diffusion on a heterogeneous GB network comprising boundaries with two distinct diffusivities and assessed the accuracy of effective medium approximations in determining an effective diffusivity. More recently, using a similar approach, Li and Holland[15] examined the interplay between network topology and boundary character, as described by two distinct GB diffusion coefficients. While this work provides an important connection between boundary structure and measurable kinetic properties, it is also desirable to link the effective diffusivity to realistic GB character distributions and to examine the temperature dependence of the activation energy for diffusion to identify diffusive regimes and to quantify deviations from Arrhenius behavior.

In this paper, we assess the impact of GB variability on mass transport in two models of a polycrystal by employing both numerical and analytical methods to extract an effective diffusivity from a steady-state diffusion profile. We consider both idealized cases in which the spectrum of GB diffusivities is discrete and the case in which there is a continuous spectrum of diffusivities. In this latter case, we link the distribution of boundary diffusivities to experimentally obtained GB character data and determine the effective diffusivity for two prototypical microstructures. The dependence of the corresponding effective activation energies on temperature is also calculated and compared to standard Arrhenius behavior. Finally, we examine the impact of a GB complexion transition on diffusion in a polycrystal.

This paper is organized as follows. In Sec. II, we outline our simulation methodology for solving the steady-state diffusion equation. In Sec. III, we discuss two major factors controlling polycrystalline diffusion response, namely, the variability of boundary structure and microstructural geometry. In Sec. IV, we highlight our analytical results for a

simple microstructure comprising parallel boundary and our numerical results for Voronoi microstructures. Section V contains a brief summary of the main findings of this work and a discussion of related issues.

II. SIMULATION METHODOLOGY

Steady-state GB diffusion in a two-dimensional system having a polycrystalline microstructure is modeled here by employing a control-volume based, finite-difference method to solve numerically for the concentration field, $c(\vec{r})$, as a function of position $\vec{r}$. For this inhomogeneous system in a cell of size $\ell \times \ell$, one can regard the isotropic diffusivity, $D(\vec{r})$, as a function of $\vec{r}$. The determination of an effective diffusivity, D_{eff}, for the system begins with the assignment of diffusivities and initial concentrations to both lattice and GB sites of a square lattice, along with the imposition of the Dirichlet boundary conditions $c(y = 0) = 1$ and $c(y = \ell) = 1$ and the Neumann conditions $(\partial c/\partial x)(x = 0) = (\partial c/\partial x)$ $(x = \ell) = 0$ (see Fig. 1). Standard central-difference methods[16] are then used to discretize the differential equation

$$\vec{\nabla} \cdot [D(\vec{r})\vec{\nabla}c(\vec{r})] = 0, \tag{1}$$

and a tridiagonal matrix algorithm is employed to obtain a numerical solution.[17] After convergence to the steady-state concentration profile $c_{ss}(\vec{r})$, the corresponding flux vector, $\vec{J}(\vec{r}) = -D(\vec{r})\vec{\nabla}c_{ss}(\vec{r})$, is calculated for every control volume. The effective diffusivity is then obtained by first performing an area average of the flux to obtain

$$D_{eff} = \ell \langle \vec{J}(\vec{r}) \rangle \cdot \hat{y}, \tag{2}$$

where the angle brackets denote an average over the area of the system.[18]

We will consider here two prototypical microstructures, namely, a series of parallel boundaries and a polycrystal comprising Voronoi grains. These two characteristic structures are shown in Figs. 2(a) and 2(b), respectively. The former structure is consistent with parallel transport and will be discussed in more detail below. The
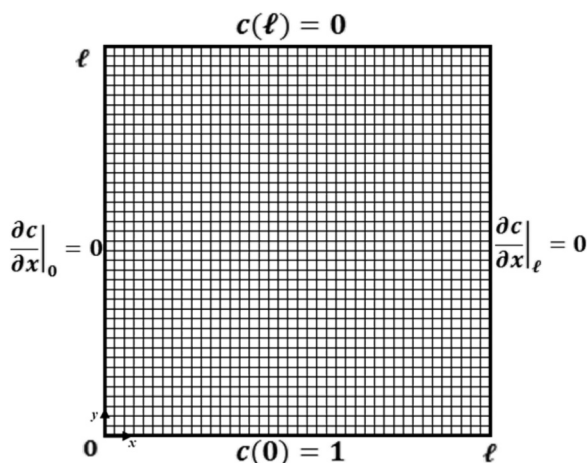

FIG. 1. A schematic of the simulation cell showing the location of the applied boundary conditions.
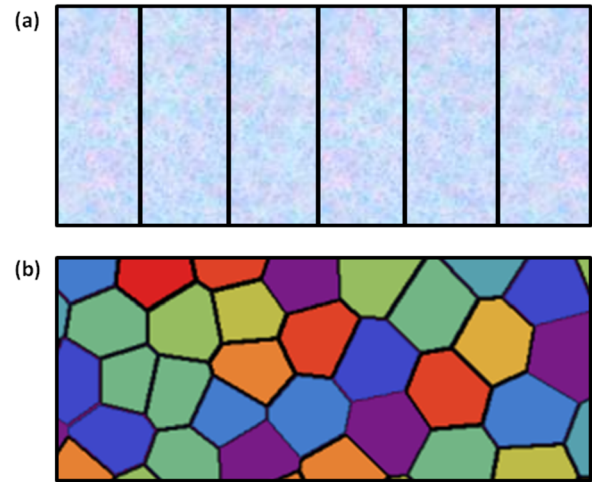

FIG. 2. Two prototypical microstructures used to calculate an effective diffusivity, D_{eff}. (a) A parallel arrangement of grain boundaries (shown in black). In general, each boundary has a different diffusivity. (b) A Voronoi microstructure resulting from randomly distributed generators.

microstructure shown in Fig. 2(b) was generated from a centroidal Voronoi tessellation (CVT) algorithm comprising 100 generators.[19] By contrast with the standard Voronoi tessellation based on randomly distributed generators, the CVT is constructed from generators that are the mass centroids of the resulting grains. Consequently, the CVT algorithm leads to a more uniform distribution of nearly-equiaxed grains. In our discretized representation, the grain boundaries of this microstructure are matched with a group of lattice sites such that neighboring control volumes share at least one side. Moreover, grain boundaries are assigned widths of at most three control volumes. To obtain statistically meaningful results, $D_{eff}(T)$ at a temperature T is averaged over approximately 50 independent microstructures, each having the same number of generators. Finally, the corresponding effective activation energy is obtained by differentiation from the relation $Q_{eff}(T) = -k_B \partial \ln(D_{eff})/\partial(1/T)$.

III. POLYCRYSTALLINE MASS TRANSPORT

As indicated above, mass transport in polycrystals is a complex phenomenon owing to several factors, including the variability of GB activation energies and the connectivity of the GB network. The interplay between these factors determines the effective diffusivity of the system and its dependence on temperature, stress, etc. In this section, we first outline two descriptions of boundary kinetics in terms of the probability density of the boundary activation energy. While these models are necessarily idealized, a connection will be made with experimental data. We next highlight two prototypical microstructural models that constitute a collection of interconnected, fast diffusive pathways surrounded by a bulk region. For these models, we obtain approximate analytical expressions for the effective diffusivity. In the Sec. IV, we determine $D_{eff}(T)$ for the two prototypical microstructures using the aforementioned kinetic models to describe the distribution of activation energies.

A. Variability of activation energies

As noted above, in most treatments of GB diffusion in polycrystals, one makes the simplifying assumption that all boundaries have the same diffusivity and, hence, identical activation energies for diffusion.[4,5] While this assumption makes subsequent analyses tractable, in reality there is a distribution of GB character, and therefore a spectrum of diffusivities and associated activation energies, $Q_{GB}^{(i)}(i = 1, 2, \ldots, N_0)$, for the N_0 grain boundaries comprising a given microstructure. Thus, it is useful to regard the activation energy for diffusion, Q, as a continuous random variable with a corresponding density of states, $N(Q)$, and an associated probability density function, $p(Q)$. For example, a discrete model of microstructural kinetics having n GB activation energies and a bulk (B) activation energy, Q_B, would take the form

$$p(Q) = f_B \delta(Q - Q_B) + \sum_i^n f_i \delta(Q - Q_{GB}^{(i)}), \quad (3)$$

where f_i is the volume fraction of GB sites, f_B is the volume fraction of bulk sites, and $\delta(Q)$ is the Dirac delta function. These volume fraction variables obey the constraint $f_B + \sum_i f_i = 1$. This simplified kinetic model will be considered in some detail below.

A more realistic, continuous model for GB diffusion must account for the microstructural complexity of a polycrystal. Consider the distribution of GB energy, γ, for a ferritic steel, as obtained by Beladi and Rohrer,[20] shown in Fig. 3. In the following development, we will formulate a general continuous model and neglect, to a first approximation, the temperature dependence of γ. One can approximate the logarithmic dependence of boundary population on γ shown in the figure by defining a GB population, $N(\gamma)$, such that the associated population density

$$\bar{p}(\gamma) = \frac{\bar{N}(\gamma)}{\int_{\gamma_{min}}^{\gamma_{max}} d\gamma \bar{N}(\gamma)} = b \exp(-\alpha\gamma), \quad (4)$$

where α is the (temperature-dependent) slope of the plot, b is a constant, and γ_{min} (γ_{max}) is the minimum (maximum) GB
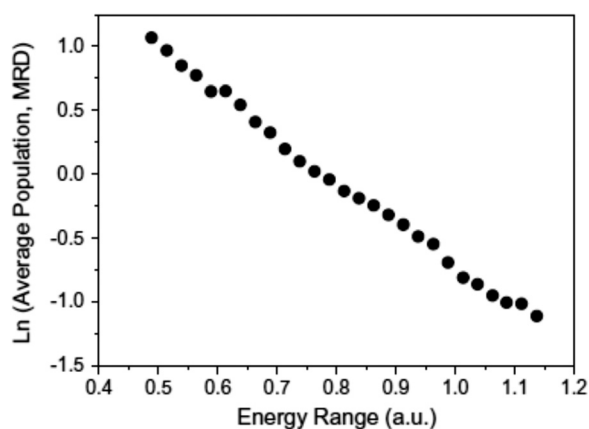

FIG. 3. The logarithm of the number of grain boundaries as a function of GB energy, γ, for a ferritic steel, as obtained from Ref. 20. Reprinted with permission from H. Beladi and G. S. Rohrer, Acta Mater. **61**(4), 1404–1412 (2013). Copyright 2013 Elsevier.

energy in the range considered. Proper normalization of this density leads to

$$\bar{p}(\gamma) = \frac{\bar{N}(\gamma)}{N_0} = \left[\frac{1}{\exp(-\alpha\gamma_{min}) - \exp(-\alpha\gamma_{max})}\right] \exp(-\alpha\gamma), \quad (5)$$

where the total number of boundaries $N_0 = \int_{\gamma_{min}}^{\gamma_{max}} d\gamma \bar{N}(\gamma)$.

The distribution of GB energies can be related to the distribution of GB activation energies for diffusion by employing an empirical relation due to Borisov that relates γ to the GB activation energy, Q_{GB}, at a temperature T.[21–24] This relation can be written conveniently as

$$\gamma = \left(\frac{1}{2a^2}\right)\left[k_B T \ln\left(\frac{D_{0GB}}{D_{0B}}\right) + (Q_B - Q_{GB})\right], \quad (6)$$

where a is the average atomic distance and D_{0GB} (D_{0B}) is the diffusional prefactor for a GB (the bulk). Given the Borisov relation, one can now perform a transformation of variables to obtain using Eq. (5)

$$\begin{aligned}
p(Q) = &\left[\frac{\kappa f}{\exp(\kappa Q_{GB}^{max}) - \exp(\kappa Q_{GB}^{min})}\right] \\
&\times \exp(\kappa Q)\Theta(Q - Q_{GB}^{min})\Theta(Q_{GB}^{max} - Q) \\
&+ f_B \delta(Q - Q_B), \quad (7)
\end{aligned}$$

where f is the GB fraction, $\kappa = \alpha/2a^2$, $\Theta(Q_{GB})$ is a step function, and

$$\begin{aligned}
Q_{GB}^{max} &= -2a^2\gamma_{min} + k_B T \ln\left(\frac{D_{0GB}}{D_{0B}}\right) + Q_B, \\
Q_{GB}^{min} &= -2a^2\gamma_{max} + k_B T \ln\left(\frac{D_{0GB}}{D_{0B}}\right) + Q_B.
\end{aligned} \quad (8)$$

In the discussion below, we will calculate an effective diffusivity based on this relation as a function of the distribution width parameter $\Delta Q = Q_{GB}^{max} - Q_{GB}^{min}$.

B. Microstructural models

Given the probability density for Q, $p(Q)$, one can obtain an approximate expression for the effective diffusivity, $D_{eff}(T)$, for a particular microstructure. As noted above, we will consider two special cases here, namely, a parallel arrangement of boundaries and a CVT microstructure constructed from a collection of distributed generators. These prototypical microstructures are shown in Figs. 2(a) and 2(b), respectively.

1. Independent, parallel grain boundaries

To a good approximation, the diffusion kinetics associated with the microstructure in Fig. 2(a) is describable in terms of parallel transport processes. This approximation is valid to the extent that the different boundary regions are independent and, hence, when the boundary separation is relatively large. Thus, for a common prefactor, D_0, one may write that[25,26]

$$D_{eff}(T) = \frac{D_0}{N_0} \int_0^\infty dQ N(Q) \exp\left(-\frac{Q}{k_B T}\right), \qquad (9)$$

and identify a corresponding effective activation energy

$$Q_{eff}(T) = \frac{\int_0^\infty dQ Q N(Q) \exp\left(-\frac{Q}{k_B T}\right)}{\int_0^\infty dQ N(Q) \exp\left(-\frac{Q}{k_B T}\right)}. \qquad (10)$$

The effective diffusivity, $D_{eff}(T)$, plays the role of the classical partition function in statistical mechanics[27] in this context, an analogy that will be exploited further below.

2. Centroidal Voronoi microstructure

For the case of the CVT shown in Fig. 2(b), it is useful to obtain analytically an approximate value for D_{eff}. For this purpose, one can regard this system as a composite medium comprising elements having different kinetic properties. As such, there are several approaches that can be taken to determine D_{eff}, including the establishment of rigorous bounds[28] and the use of a Maxwell-Garnett effective-medium artifice.[29,30] Following the Maxwell-Garnett approach as applied to mass transport,[31] an approximation for D_{eff} can be obtained as follows. For a system with a single GB diffusivity, D_{GB}, one can approximate the medium as a collection of bulk (grain interior) regions embedded in a GB matrix (see Fig. 4). This assignment of regions is advantageous as it creates a series of spatially compact domains surrounded by a common matrix. By solving for the steady-state concentration fields in the bulk, matrix, and embedded medium, one obtains, in two dimensions,

$$D_{eff} = D_{GB}\left[1 + \frac{2(1-f)(D_B - D_{GB})}{D_B + D_{GB} - (1-f)(D_B - D_{GB})}\right], \quad (11)$$

where f is the GB area fraction.

For systems having more than one GB diffusivity, we have devised a new approach here. More specifically, one can proceed as described above, except that one must define D_{GB} to reflect the spectrum of GB diffusivities. Two prescriptions were employed for this purpose. The first prescription assumes that there is a mixture of GB diffusivities
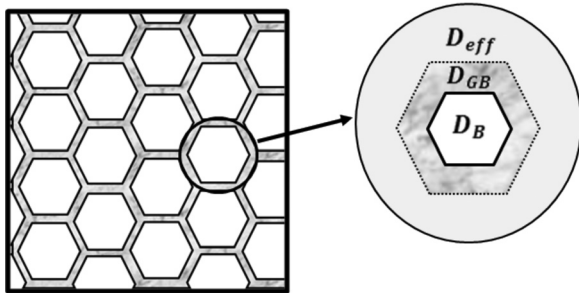

FIG. 4. A schematic of an idealized microstructure showing the geometry associated with the Maxwell-Garnett calculation of D_{eff}. The matrix phase comprises the grain boundaries, having a diffusivity D_{GB}, while the embedded phase corresponds to the grain interiors, having a diffusivity D_B. The effective diffusivity, D_{eff}, is obtained by solving the steady-state diffusion equation subject to the appropriate boundary conditions at the bulk/boundary and boundary/effective medium interfaces.

outside the percolation regime. Following Kirkpatrick,[30] one finds, for a square lattice, that:

$$\int dD'_{GB} \frac{D'_{GB} - D_{GB}}{D'_{GB} + D_{GB}} p(D'_{GB}) = 0, \qquad (12)$$

where $p(D'_{GB})$ is the probability density function for the GB diffusivity. For a given probability density function, Eq. (12) can be solved for D_{GB} for use in Eq. (11). The second prescription, due to Hart,[32] assumes that the GB diffusivities can be combined independently. Thus, for two diffusivities,

$$D_{GB}(T) = \left[f_1 D_{0GB}^{(1)} \exp\left(-\frac{Q_{GB}^{(1)}}{k_B T}\right) + f_2 D_{0GB}^{(2)} \exp\left(-\frac{Q_{GB}^{(2)}}{k_B T}\right)\right], \qquad (13)$$

where $D_{0GB}^{(1)}$ and $D_{0GB}^{(2)}$ are the diffusional prefactors for the two boundaries. The values of D_{GB} calculated using Eq. (13) can again be used in Eq. (11). Both prescriptions will be employed to interpret our results, as described below.

IV. RESULTS

A. Analytical results—Parallel boundaries

1. Two boundary types

We first examine the case of diffusion in a system comprising parallel grain boundaries, as shown in Fig. 2(a). As noted above, in the limit that the GB diffusivities are much larger than the bulk diffusivity, the boundaries constitute nearly independent, fast diffusive pathways. Thus, in this limit, we can calculate D_{eff} directly from Eq. (9) without appealing to numerical methods. As an example, consider two distinct GB boundary types, with corresponding activation energies $Q_{GB}^{(1)}$ and $Q_{GB}^{(2)}$ and volume fractions f_1 and f_2. The effective diffusivity, found using Eq. (3), is

$$D_{eff}(T) = D_0 \left[f_B \exp\left(-\frac{Q_B}{k_B T}\right) + f_1 \exp\left(-\frac{Q_{GB}^{(1)}}{k_B T}\right)\right.$$
$$\left. + f_2 \exp\left(-\frac{Q_{GB}^{(2)}}{k_B T}\right)\right]. \qquad (14)$$

Figure 5(a) shows the dependence of the logarithm of $D_{eff}(T)$ on $1/T$ for the case of two distinct boundaries with coefficients given by $f_B = 0.5$, $f_1 = 0.05$, and $f_2 = 0.45$ and corresponding activation energies $Q_B = 1.0\,\mathrm{eV}$, $Q_{GB}^{(1)} = 0.1\,\mathrm{eV}$, and $Q_{GB}^{(2)} = 0.35\,\mathrm{eV}$. For this parameter set, there are broadly two diffusive regimes, as determined by the relative activation energies and the relative volume fraction of sites. This behavior is characteristic of kinetic quantities in systems having different activation energies, such as diffusion in polycrystalline silver[33] and the electrical conductivity of an extrinsic semiconductor.[34] The effective activation energy is displayed in Fig. 5(b). It is evident that there are, broadly speaking, two regimes characterized by different activation energies. In Fig. 5(c), the temperature derivative $C = dQ_{eff}/dT$ is shown as a function of T. This quantity plays a role analogous to the heat capacity in statistical physics and exhibits a "Schottky" peak

that is characteristic of multi-level systems. Indeed, from the location of this peak, one can define a transition temperature, $T_K \approx 800\,\text{K}$, separating the two kinetic regimes. More generally, the shape of this peak embodies information about the spectrum of activation energies that characterizes this system.

2. Continuous distribution of activation energies

For the continuous distribution of activation energies given in Eq. (7), one can calculate D_{eff} using Eq. (9). Upon substituting Eq. (7) into Eq. (9), one obtains

$$D_{eff}(T) = D_0 \left\{ \left(\frac{f_1 \sigma}{\sigma - \epsilon} \right) \left[\frac{\exp(\sigma - \epsilon) - 1}{\exp(\sigma) - 1} \right] \right.$$
$$\left. \times \exp\left(-\epsilon \bar{Q}_{GB}\right) + f_B \exp\left(-\epsilon \bar{Q}_B\right) \right\}, \qquad (15)$$

where the dimensionless parameters are $\sigma = \kappa \Delta Q$, $\epsilon = \Delta Q / k_B T$, $\bar{Q}_{GB} = Q_{GB}^{min} / \Delta Q$, and $\bar{Q}_B = Q_B / \Delta Q$. We note that Nicholas found a similar expression for an effective reaction rate when considering the problem of parallel activated processes involving multiple catalytic sites.[25] Before examining the corresponding $Q_{eff}(T)$, it is useful to obtain first the normalized, relative activation energy, calculated using Eq. (15), in the somewhat artificial, boundary-dominated limit $f_B/f_1 \to 0$. One finds that

$$\bar{Q}_{eff} = \frac{Q_{eff} - Q_{GB}^{min}}{\Delta Q} \to \frac{1}{\epsilon - \sigma} + \frac{1}{1 - \exp(\epsilon - \sigma)}. \qquad (16)$$

In the zero-temperature limit, $(\epsilon \to \infty)\, \bar{Q}_{eff} \to 0$ for σ finite, while in the high-temperature limit $(\epsilon \to 0)\, \bar{Q}_{eff} \to 1/2$ as $\sigma \to 0$ and $\bar{Q}_{eff} \to 1$ as $\sigma \to \infty$. Thus, if there is little variability in the distribution of GB activation energies over a range of width ΔQ, Q_{eff} increases by an amount approximately equal to the average of Q_{GB}^{max} and Q_{GB}^{min} at high temperatures. If, however, there is substantial variability in the distribution of activation energies, then Q_{eff} varies over the full range from Q_{GB}^{min} to Q_{GB}^{max} as the temperature increases.

In most cases, however, the behavior outlined above is masked by bulk diffusion due to the high volume fraction of bulk sites. At nanocrystalline length scales, however, where the volume fraction of grain boundaries can be 50%,[35] one expects a competition between GB and bulk diffusion. Figure 6 shows the dependence of $\bar{Q}_{eff}$ on ϵ (temperature) for three different values of σ for the case that $f_B/f_1 = 1$ and a normalized bulk activation energy $\bar{Q}_B = 3.0$. As expected, at high temperatures, $\bar{Q}_{eff}$ saturates at a value somewhat above that in the boundary-limited case since bulk diffusion is operative at these temperatures.

B. Simulation results—Centroidal Voronoi microstructure

For the case of a CVT, as shown in Fig. 2(b), we obtain D_{eff} by numerical solution of the steady-state diffusion equation, as outlined above. We also assess various effective-medium approximations formulated to describe the diffusive
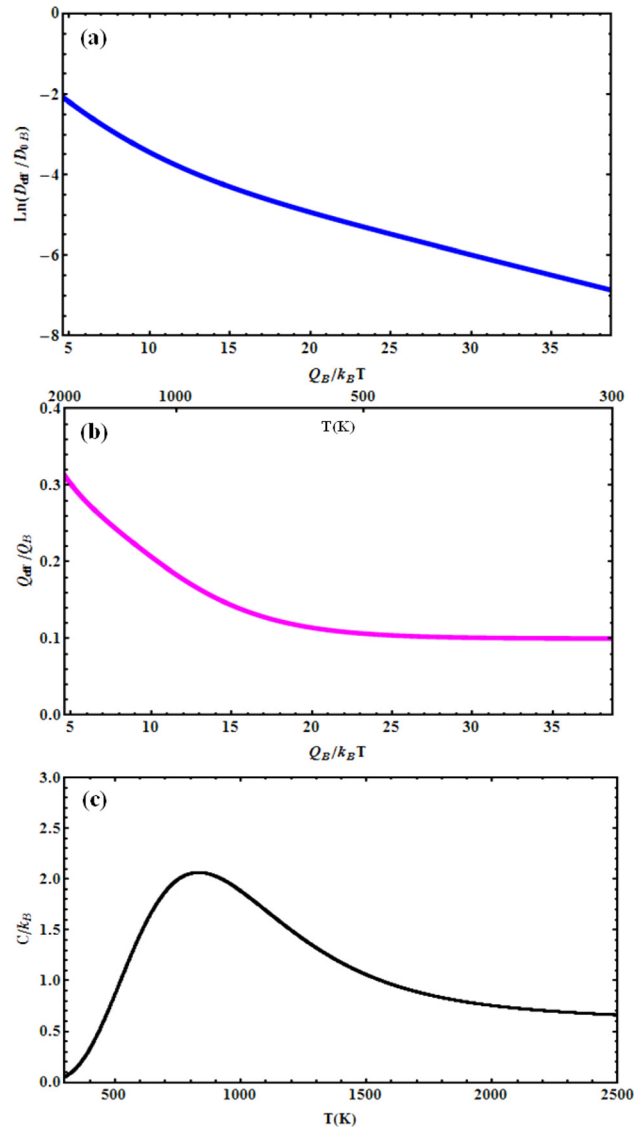

FIG. 5. (a) The logarithm of $D_{eff}(T)/D_{0B}$ versus inverse temperature, $Q_B/k_B T$, for the case of two distinct boundaries with volume fractions given by $f_B = 0.5$, $f_1 = 0.05$, and $f_2 = 0.45$ and corresponding activation energies $Q_B = 1.0$, $Q_{GB}^{(1)} = 0.1$, and $Q_{GB}^{(2)} = 0.35$ (in units of eV). (b) The effective activation energy, Q_{eff}/Q_B, versus temperature, T, for this case. (c) The quantity $C/k_B = dQ_{eff}/dT$ versus temperature, T, where k_B is Boltzmann's constant. Note the peak that is characteristic of multi-state systems.

response of these systems. Given our focus on the steady state, each side of Eq. (1) can be divided by D_{0B}, and so only the ratios of prefactors are relevant here. Also, for concreteness, we fix the bulk activation energy $Q_B = 1.0\,\text{eV}$. For this microstructure, we investigate the transport behavior for three different scenarios, namely: (1) two types of boundaries (i.e., boundaries having different activation energies and diffusional prefactors), (2) a system undergoing a complexion transition in which a fraction of the boundaries transforms at a temperature T_t, and (3) boundaries having a spectrum of activation energies distributed according to Eq. (7). Rather than explore a wide range of parameter space, we focus here on a few illustrative cases that exhibit different diffusive regimes.
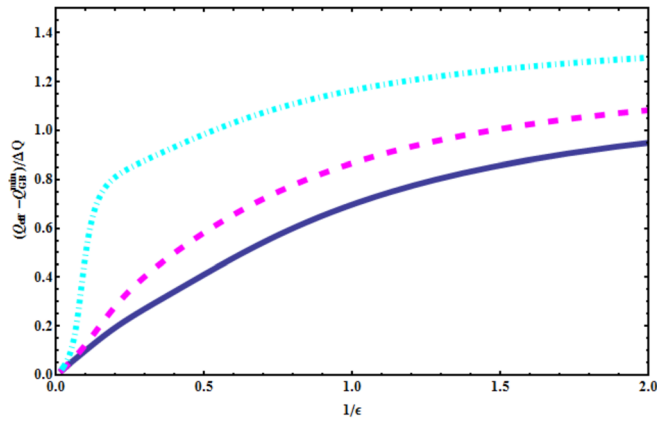
FIG. 6. The dependence of the normalized, effective activation energy $\bar{Q}_{eff} = (Q_{eff} - Q_{GB}^{min})/\Delta Q$ on ϵ for $\sigma = 0.01$ (solid line), 2.0 (dashed line), and 10.0 (dotted-dashed line). The ratio of bulk to GB volume fractions is $f_B/f_1 = 1$, and the normalized bulk activation energy $\bar{Q}_B = 3.0$.

1. Scenario 1: Two types of boundaries

In this scenario, two *distinct* grain boundary types, with diffusivities described by different activation energies and prefactors, comprise the microstructure. The goal here is to investigate the role of boundary type in determining the effective diffusivity. We consider two cases, with the corresponding parameter sets summarized in Table I. In each case, the total volume fraction of boundary sites is 0.105. The first case corresponds to a typical situation in which grain boundaries constitute high-diffusivity paths (with relatively low associated activation energies) relative to the bulk owing to their relatively open structure. By contrast, the second case corresponds to a situation in which the GB activation energies exceed that of the bulk. While this situation may be somewhat counterintuitive as it does not occur in metals, larger activation energies for GB diffusion have been reported for some ceramic systems.[36] For this latter case, the effective diffusivity is dominated by grain boundaries at high temperatures, while for low temperatures, bulk diffusion is found to be dominant for the choice of model parameters given in Table I.

For the first case, Fig. 7(a) shows the dependence of $D_{eff}(T)$ on inverse temperature as obtained from numerical solution of the steady-state diffusion equation and from two implementations of effective medium theory. Figure 7(b) shows the dependence of the associated effective activation energy, $\bar{Q}_{eff}(T)$, on temperature, T. More specifically, D_{GB} is calculated in two different ways, using either the Kirkpatrick (see Eq. (12)) or the Hart (see Eq. (13)) approach. D_{eff} is then obtained for each case by substituting D_{GB} into

TABLE I. A summary of the kinetic parameters for the two cases comprising scenario 1. The total volume fraction of boundary sites is 0.105 with approximately 40% of the boundaries being type 1.

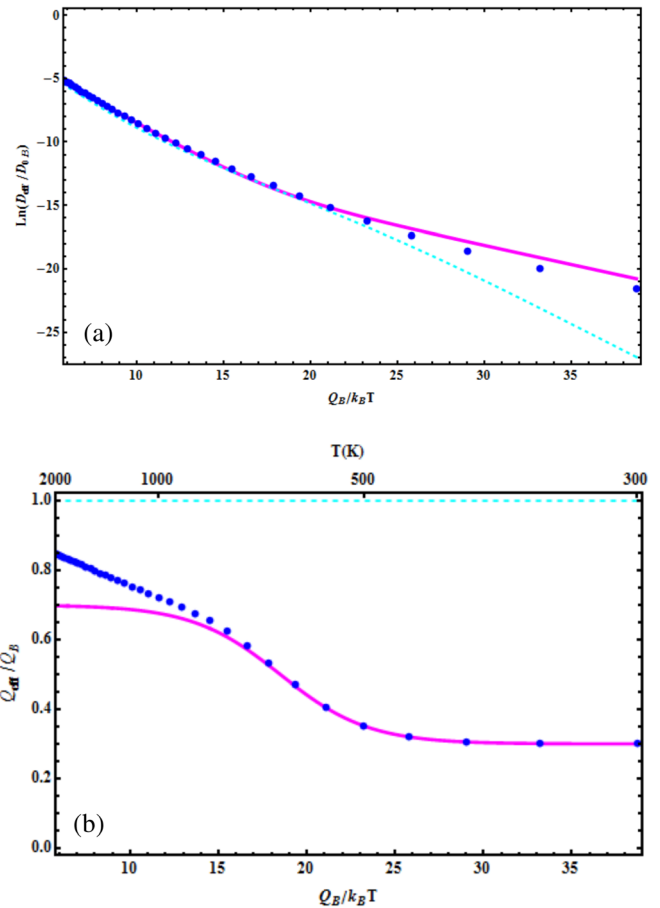|	Case 1	Case 2
$Q_{GB}^{(1)}/Q_B$	0.3	1.5
$Q_{GB}^{(2)}/Q_B$	0.7	1.25
$D_{0GB}^{(1)}/D_{0GB}^{(2)}$	0.0001	100

FIG. 7. (a) The dependence of the logarithm of the effective diffusivity, $D_{eff}(T)/D_{0B}$, on inverse temperature, Q_B/k_BT, for case 1 (scenario 1) as determined by the solution of the steady-state diffusion equation (circles) and from the Kirkpatrick (dashed line) and Hart (solid line) effective medium theories. (b) The associated effective activation energy Q_{eff}/Q_B as a function of temperature, T (circles). Also shown is the GB contribution to Q_{eff}, calculated using the Hart approach (solid line), and the bulk contribution to Q_{eff} (dotted line). Note that there are, broadly speaking, two distinct diffusive regimes.

Eq. (11). As is evident from Fig. 7(a), at high temperatures both implementations reproduce the numerical data well, while at low temperatures, the use of Eq. (13) in the effective medium approximation is superior. Moreover, the temperature dependence of $\bar{Q}_{eff}(T)$ highlights two diffusive regimes with a kinetic transition temperature at $T_K \approx 600$ K. The low-temperature regime is dominated, as expected, by the grain boundaries.

For the second case, Fig. 8(a) shows the dependence of $D_{eff}(T)$ on inverse temperature as obtained from numerical solution of the steady-state diffusion equation, by the Maxwell-Garnett effective medium theory (with the Hart approach) and by a hybrid approach described below. The use of the standard Maxwell-Garnett effective medium theory is not wholly adequate here, as indicated in the figure. The reason for this inadequacy is that the large volume fraction of bulk sites employed here and the higher bulk diffusivity imply that the bulk phase, rather than the grain boundaries, should be considered as the matrix phase at low temperature. Thus, one can apply the Maxwell-Garnett approach as before in the high-temperature regime, while in the low-temperature
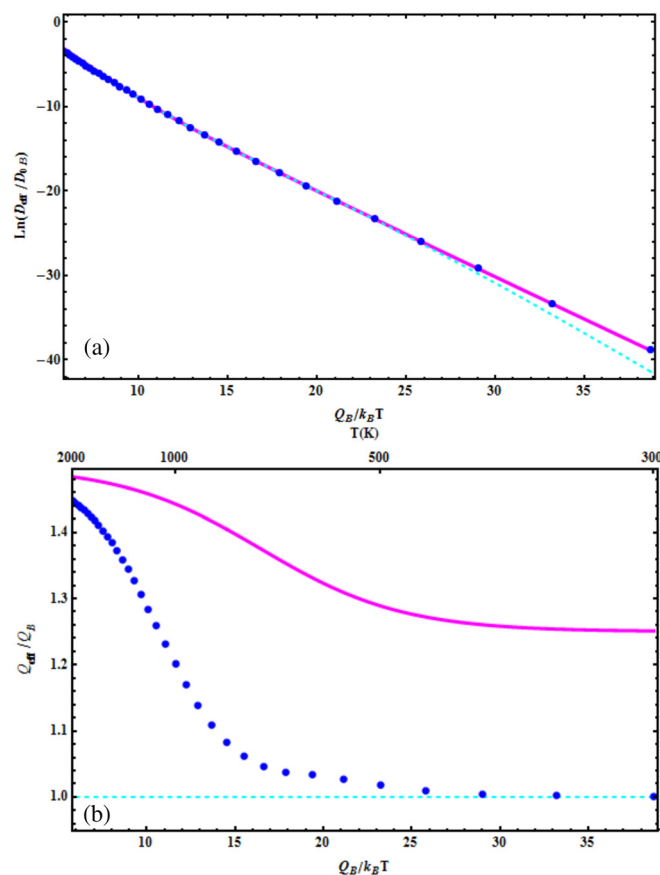
FIG. 8. (a) The dependence of the logarithm of the effective diffusivity, $D_{eff}(T)/D_{0B}$, on inverse temperature, Q_B/k_BT, for case 2 (scenario 1) as determined by the solution of the steady-state diffusion equation (circles). Also shown are the results of the hybrid effective medium theory (solid line) and the conventional Maxwell-Garnett approach (dashed line). (b) The associated effective activation energy $\bar{Q}_{eff}/Q_B$ as a function of temperature, T (circles). Also shown is the GB contribution to $\bar{Q}_{eff}$, calculated using the Hart approach (solid line), and the bulk contribution to $\bar{Q}_{eff}$ (dotted line).

regime, one should interchange the roles of GB and bulk. The resulting hybrid effective medium theory is seen to reproduce the data well over the wide range of temperatures considered here. Figure 8(b) shows the dependence of the associated effective activation energy, $\bar{Q}_{eff}$, on temperature. It should be noted that by contrast with the previous case, the low-temperature regime is dominated by bulk kinetics, while the high-temperature regime reflects grain-boundary kinetics. This dominance of bulk kinetics at low temperatures follows from the choice of parameters given in Table I.

2. Scenario 2: Complexion transition

In this scenario, a fraction of the boundaries undergoes a complexion transition as a function of temperature. A complexion transition is similar in many respects to a phase transition. However, since a phase is homogeneous according to the strict Gibbsian definition, we employ the term complexion to describe interfacial material of finite thickness in equilibrium with an abutting phase whose existence requires the presence of the abutting phase. Moreover, this interfacial material need not have the same structure or composition as that

TABLE II. A summary of the kinetic parameters for scenario 2. The total volume fraction of boundary sites is 0.105 with approximately 40% of the boundaries being type 1. The complexion transition temperature is $T_t = 700 \, \mathrm{K}$.

	GB 1	GB 2
Q_{GB}/Q_B	0.3	0.7
D_{0GB}/D_{0B}	0.0005	5.0 $(T < T_t)$, 50.0 $(T \geq T_t)$

of the abutting phase. As discussed above, such complexion transitions involve structural and chemical changes at a boundary, and therefore have implications for boundary kinetics.[2]

Previous studies have led to the identification of a series of complexion types and the realization that property changes, such as changes in GB mobility or embrittlement,[37] are associated with complexion transitions.[38] In this case, it is assumed that changes in GB diffusion attend these structural and chemical changes at interfaces. For simplicity, we again consider two *distinct* GB types having the parameter set summarized in Table II. For temperatures below T_t, this set corresponds to that for case 1 of scenario 1. To model a complexion transition, it is assumed that a transition occurs at a temperature $T_t = 700 \, \mathrm{K}$, and that there is an associated change in the diffusional prefactor corresponding to one of the grain boundaries. This model is consistent with the observations of Dillon *et al.*[39] that GB mobilities in doped and undoped alumina exhibit distinct kinetic regimes that are associated with different complexions. Moreover, an Arrhenius analysis of the temperature dependence of the mobilities for these regimes showed that, while their activation energies were quite similar, each had a different kinetic prefactor.

Figure 9 displays the dependence of $D_{eff}(T)$ on inverse temperature as obtained from numerical solution of the steady-state diffusion equation and, in addition, as calculated using both the Kirkpatrick and the Hart effective medium theories. As is evident from the figure, the Hart approach
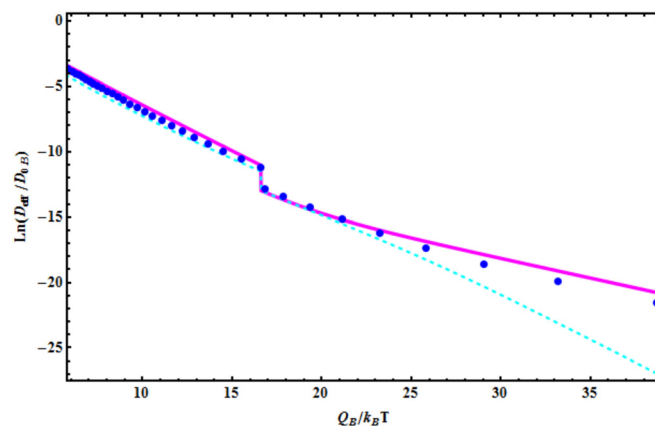

FIG. 9. The dependence of the logarithm of the effective diffusivity, $D_{eff}(T)/D_{0B}$, on inverse temperature, Q_B/k_BT, as obtained from numerical solution of the steady-state diffusion equation (circles) and, in addition, as calculated using both the Kirkpatrick (dashed line) and the Hart (solid line) effective medium theories.
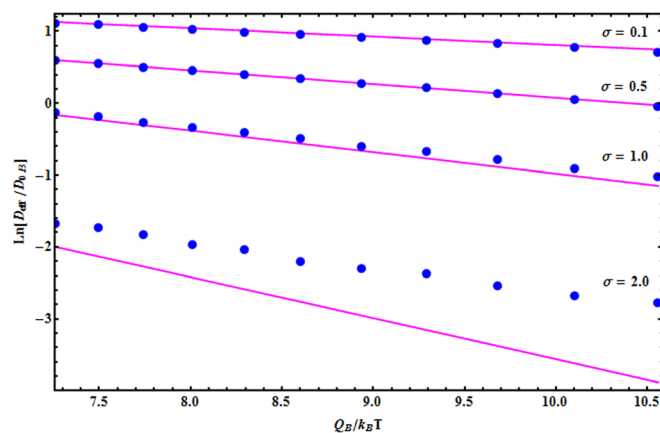
FIG. 10. The logarithm of D_{eff}/D_{0B} as a function of Q_B/k_BT for various values of σ for a continuous distribution of GB activation energies. The solid lines represent the simulation results and the dashed lines are calculated using effective medium theory.

again captures the diffusive response over a wide range of temperatures. Moreover, there is a jump in the value of D_{eff} due to a change in a GB diffusional prefactor at T_t. This jump in the effective diffusivity translates into an increase in Q_{eff} at the same temperature. Thus, one must be careful in the interpretation of such plots to determine whether a change in Q_{eff} is due to a change in activation barriers or, as in this scenario, a change in attempt frequencies (i.e., prefactors). More generally, one would expect that different boundary types would have one or more different complexion transition temperatures, and so the sharp jump evident in Fig. 9 would be replaced by a smoother transition.

3. Scenario 3: Continuous distribution of activation energies

In this scenario, the activation energy for a given boundary is drawn from the distribution of activation energies given in Eq. (7). To draw from this distribution, one generates a uniform deviate and, from the logarithm of this deviate, obtains the desired exponentially distributed random variable.[16] The diffusivities obtained in this manner are then randomly assigned to the grain boundaries in the system. For this distribution of activation energies, we performed several simulations for different values of ΔQ at a fixed value of $\kappa = 3.0\,\text{eV}^{-1}$. This value of κ was determined from the slope of the plot in Fig. 3, assuming that a typical value for the maximum γ is about $1.0\,\text{J/m}^2$. The results from the aforementioned simulations are displayed in Fig. 10, which shows $\ln(D_{eff}/D_{0B})$ as a function of Q_B/k_BT for several different values of $\sigma = \kappa\Delta Q$. Also shown are the predictions of effective medium theory, obtained by using the Kirkpatrick approach (Eq. (12)) to calculate D_{GB} for use in Eq. (11). As can be seen from the figure, effective medium theory reproduces much of the simulation data, especially at small σ. This agreement for small σ is intuitively reasonable since the effective medium approximation should work best for a single activation energy or, in general, for a very narrow range of activation energies.

V. DISCUSSION AND CONCLUSIONS

In this work, we employed both analytical and numerical methods to examine the impact of GB variability (i.e., a spectrum of boundary activation energies) on diffusion in a polycrystal. In particular, we calculated an effective diffusivity, D_{eff}, and associated activation energy, Q_{eff}, as a function of temperature for different microstructures using simplified, multi-state models and models based on an experimentally obtained GB energy distribution. The main conclusions of this study are as follows:

(1) The variability in polycrystalline GB character leads, via the Borisov relation, to a probability density for GB activation energies and an associated effective diffusivity that can be characterized by a few parameters.
(2) From the effective diffusivity, one can obtain a temperature dependent effective activation energy by differentiation. An analysis of this activation energy can be used to identify different diffusive regimes and associated transition temperatures.
(3) Effective medium theory can be generalized to incorporate both bulk and multiple GB diffusivities. This theory describes the effective diffusivity in many polycrystalline systems over a wide range of temperatures.
(4) Complexion transitions affect the spectrum of GB activation energies, and one can assess their impact on GB diffusion using the numerical procedure described above.

Several extensions of this work are currently underway. First, it is of interest to determine how microstructural descriptors, such as grain size and shape, affect D_{eff}. With regard to grain size, stereological arguments can be used to estimate the fraction of GB sites. For example, for a Poisson Voronoi structure, the average GB perimeter per grain is $4/\sqrt{\rho}$, where ρ is the areal grain density.[40] Thus, it is straightforward to estimate the fraction of boundary sites for a fixed number of grains. Second, as indicated above, the assignment of activation energies to boundaries in this work was, for simplicity, taken to be random. In reality, one would expect GB properties to be spatially correlated, and it would therefore be of interest to examine quantitatively how spatial correlations influence D_{eff}. This may be accomplished by introducing a correlation length in the distribution of GB diffusivities that would extend no more than one or two average grain diameters. Third, it has been assumed here that the kinetic attributes of a given boundary are spatially uniform and isotropic. This assumption is clearly an idealization as real boundaries will exhibit some nonuniformity and anisotropy in properties. For example, to model a spatially diffuse boundary, one can incorporate a position dependent boundary diffusivity that varies from its maximum near the center of the boundary to a bulk value at a given distance from the center. In the case of a three-dimensional model of anisotropic, boundary pipe diffusion, it is also possible to assign different diffusivities in a boundary region for transport parallel and perpendicular to the boundary. Finally, in many studies of GB diffusion in polycrystals, the grains coarsen during the course of an experiment, especially at high temperatures. The introduction of grain coarsening in our model represents a significant future challenge.

[1]C.-S. Kim, Y. Hu, G. S. Rohrer, and V. Randle, Scr. Mater. **52**, 633–637 (2005).
[2]P. R. Cantwell, M. Tang, S. J. Dillon, J. Luo, G. S. Rohrer, and M. P. Harmer, Acta Mater. **62**, 1–48 (2014).
[3]J. M. Rickman, H. M. Chan, M. P. Harmer, and J. Luo, Surf. Sci. **618**, 88–93 (2013).
[4]R. T. Whipple, Philos. Mag. **45**, 1225 (1954).
[5]T. Suzuoka, J. Phys. Soc. Jpn. **19**, 839 (1964).
[6]I. Kaur and W. Gust, *Fundamentals of Grain and Interphase Boundary Diffusion* (Ziegler Press, Stuttgart, 1988).
[7]G. H. Gilmer and H. H. Farrell, J. Appl. Phys. **47**, 3792 (1976).
[8]G. H. Gilmer and H. H. Farrell, J. Appl. Phys. **47**, 4373 (1976).
[9]J. C. Fisher, J. Appl. Phys. **22**, 74 (1951).
[10]Y. M. Mishin and C. Herzig, Philos. Mag. A **71**, 641 (1995).
[11]H. S. Levine and C. J. MacCallum, J. Appl. Phys. **31**, 595 (1960).
[12]T. P. Swiler and E. A. Holm, *Diffusion in Polycrystalline Microstructures* (Sandia National Laboratories, Albuquerque, NM, 1995).
[13]K. Bedu-Amissah, J. M. Rickman, H. M. Chan, and M. P. Harmer, J. Appl. Phys. **98**, 063511 (2005).
[14]Y. Chen and C. A. Schuh, Acta Mater. **54**, 4709–4720 (2006).
[15]L. Li and S. Holland, Nanomater. Energy **3**, 139–147 (2014).
[16]W. H. Press, B. P. Flannery, S. A. Teukolsky, and W. T. Vetterling, *Numerical Recipes: The Art of Scientific Computing* (Cambridge University Press, New York, 1989).
[17]S. Patankar, *Numerical Heat Transfer and Fluid Flow* (CRC Press, 1980).
[18]S. Prager, J. Chem. Phys. **33**, 122 (1960).
[19]Q. Du, V. Faber, and M. Gunzburger, SIAM Rev. **41**, 637 (1999).
[20]H. Beladi and G. S. Rohrer, Acta Mater. **61**(4), 1404 (2013).
[21]V. T. Borisov, V. M. Golikov, and G. V. Scherbedinskiy, Phys. Met. Metallogr. **17**, 80–84 (1964).
[22]P. Guiraldenq and P. Poyet, Mem. Sci. Rev. Metall. **70**, 715–723 (1973).
[23]T.-F. Chen, G. P. Tiwari, Y. Iijima, and K. Yamauchi, Mater. Trans. **44**, 40–46 (2003).
[24]J. Pelleg, Philos. Mag. **14**, 595–601 (1966).
[25]J. F. Nicholas, J. Chem. Phys. **31**, 922–925 (1959).
[26]M. H. Zaman, T. R. Sosnick, and R. S. Berry, Phys. Chem. Chem. Phys. **5**, 2589–2594 (2003).
[27]R. K. Pathria, *Statistical Mechanics*, 2nd ed. (Pergamon Press, New York, 1996).
[28]Z. Hashin and Z. Shtrikman, J. Appl. Phys. **33**, 3125 (1962).
[29]J. C. M. Garnett, Philos. Trans. R. Soc., A **203**, 385 (1904).
[30]S. Kirkpatrick, Rev. Mod. Phys. **45**, 574–588 (1973).
[31]D. S. McLachlan, J. Phys. C: Solid State Phys. **20**, 865 (1987).
[32]E. W. Hart, Acta Metall. **5**, 597 (1957).
[33]P. Shewmon, *Diffusion in Solids* (John Wiley and Sons, Hoboken, NJ, 1991).
[34]B. Sapoval and C. Hermann, *Physics of Semiconductors* (Springer–Verlag, New York, 1995).
[35]K. J. VanVliet, S. Tsikata, and S. Suresh, Appl. Phys. Lett. **83**, 1441–1443 (2003).
[36]A. H. Heuer, J. Eur. Ceram. Soc. **28**, 1495 (2008).
[37]A. Kundu, K. M. Asl, J. Luo, and M. P. Harmer, Scr. Mater. **68**, 146 (2013).
[38]S. J. Dillon and M. P. Harmer, J. Am. Ceram. Soc. **91**, 2304–2313 (2008).
[39]S. J. Dillon, M. Tang, W. C. Carter, and M. P. Harmer, Acta Mater. **55**, 6208 (2007).
[40]A. Okabe, B. Boots, and K. Sugihara, *Spatial Tessellations: Concepts and Applications of Voronoi Diagrams* (John Wiley, New York, 1992).